This is a repository copy of *Accounting for Nanometer-Thick Adventitious Carbon Contamination in X-ray Absorption Spectra of Carbon-Based Materials*.

Article:

Accounting for Nanometer-Thick Adventitious Carbon Contamination in X-Ray Absorption Spectra of Carbon-Based Materials

Filippo Mangolini[1], J. Brandon McClimon[1], Franck Rose[2], Robert W. Carpick[3,]*

[1] Department of Materials Science and Engineering, University of Pennsylvania, Philadelphia, Pennsylvania 19104, USA

[1] HGST, a Western Digital Company, San Jose, California 95135, USA

[3] Department of Mechanical Engineering and Applied Mechanics, University of Pennsylvania, Philadelphia, Pennsylvania 19104, USA

* Author to whom correspondence should be addressed. Electronic email: carpick@seas.upenn.edu

ABSTRACT

Near-edge X-ray absorption fine structure (NEXAFS) spectroscopy is a powerful technique for characterizing the composition and bonding state of nanoscale materials and the top few nanometers of bulk and thin film specimens. When coupled with imaging methods like photoemission electron microscopy, it enables chemical imaging of materials with nanometer-scale lateral spatial resolution. However, analysis of NEXAFS spectra is often performed under the assumption of structural and compositional homogeneity within the nanometer-scale depth probed by this technique. This assumption can introduce large errors when analyzing the vast majority of solid surfaces due to the presence of complex surface and near-surface structures such as oxides and contamination layers. An analytical methodology is presented for removing the contribution of these nanoscale overlayers from NEXAFS spectra of two-layered systems to provide a corrected photo-absorption spectrum of the substrate. This method relies on the subtraction of the NEXAFS spectrum of the overlayer adsorbed on a reference surface from the spectrum of the two-layer system under investigation, where the thickness of the overlayer is independently determined by X-ray photoelectron spectroscopy (XPS). This approach is applied to NEXAFS data acquired for one of the most challenging cases: air-exposed hard carbon-based materials with adventitious carbon contamination from ambient exposure. The contribution of the adventitious carbon was removed from the as-acquired spectra of ultrananocrystalline diamond (UNCD) and hydrogenated amorphous carbon (a-C:H) to determine the intrinsic photo-absorption NEXAFS spectra of these materials. The method alters the calculated fraction of sp^2-hybridized carbon from 5 to 20%, and reveals that the adventitious contamination can be described as a layer containing carbon and oxygen ([O]/[C]=0.11±0.02) with a thickness of 0.6±0.2 nm and a fraction of sp^2-bonded carbon of 0.19±0.03. This method can be generally

applied to the characterization of surfaces and interfaces in several research fields and technological applications.

INTRODUCTION

Near-edge X-ray absorption fine structure (NEXAFS) spectroscopy is a powerful weapon in the surface analysis arsenal thanks to its elemental specificity and its ability to obtain important information about local bonding environment, such as hybridization, chemical state, and bond orientation[1]. In addition, NEXAFS spectra can be obtained at high spatial resolution using imaging techniques such as photoemission electron microscopy[2-5] and magnetically-guided imaging[6]. The wealth of detailed information NEXAFS spectroscopy yields has made it an increasingly attractive analytical tool for several research fields, such as catalysis[7-11], tribology[6,12,13], self-assembly at surfaces[14-17], nanomaterials[18-26], and polymer science[27-32].

One of the most important applications of NEXAFS spectroscopy is the study of low atomic number (low-Z, *i.e.*, carbon, oxygen, nitrogen, and fluorine) molecules and materials[1]. The power of NEXAFS spectroscopy for investigating low-Z elements derives from the strong directionality and short length of the covalent bonds between low-Z atoms, the strong dependence of the bond length on its hybridization, and the large backscattering amplitude of low energy electrons from low-Z atoms[1]. This results in the presence of resolvable, structure-dependent resonances in NEXAFS K-edge spectra, whose intensity is strongly affected by the orientation of the final state orbital with respect to the electric field vector of the incident photon beam[1].

For carbon K-edge NEXAFS spectroscopy, in particular, the resolvable energy difference between the resonant X-ray excitations of a core-level (1s) electron to unoccupied molecular orbitals (either π^* or σ^*) allows the identification of the bonding configuration and hybridization state of carbon atoms in the near-surface region for many materials, including

diamond[6,13,21,22,24,25,33-38], diamond-like carbon[39-46], graphene[26,47,48], and polymers[27-32], as well as the determination of the surface molecular orientation of nanomaterials[18,19,49,50] and adsorbates[14-16].

Unfortunately, in addition to the typical challenges associated with the analysis of NEXAFS spectra, namely energy calibration, intensity normalization, removal of features present in as-acquired spectra due to beam instabilities, signal offsets, and the beamline transmission function[1,51,52], carbon K-edge NEXAFS spectroscopy suffers from additional difficulties. One key set of challenges derive from the presence of artifacts in the as-collected experimental data caused by the adventitious carbon contamination (subsequently modified by X-ray exposure) of X-ray optics in synchrotron beamlines[52]. Recently, Watts *et al.* reviewed and implemented the numerous methods of calibration, normalization, and artifact removal for NEXAFS spectra (with a particular focus upon carbon K-edge spectra) reported in the literature[52].

While the approaches outlined by Watts *et al.* are effective for addressing the issues commonly encountered in the evaluation of NEXAFS data[52], the corrected spectra they yield represent the photo-absorption spectra of the specimens under the assumption of structural and compositional homogeneity within the nanometer-scale depth probed by NEXAFS spectroscopy. For electron yield NEXAFS spectroscopy of low-Z elements, the information depth (the specimen thickness measured normal to the surface from which a specified percentage of typically 95% of the detected signal originates) is usually less than 5 nm[1]. Unfortunately, the assumption of chemical and structural homogeneity does not hold in the vast majority of solid surfaces due to the presence of complex surface-bound species and layers, *e.g.*, natural oxide and contamination layers[53,54]. This can lead to significant errors when analyzing elements that are simultaneously present in multiple layers. In particular, for carbon-based materials previously exposed to air, their carbon K-edge NEXAFS spectra, even when corrected using any of the approaches outlined

by Watts *et al.*[52], are a convolution of the spectrum of the sample of interest and the spectrum of the adventitious carbon contamination on its surface since the thickness of the latter (typically <2 nm[55]) is smaller than the information depth at the carbon K-edge (Figure 1). While the thickness of the adventitious carbon contamination has been shown to depend on the sample preparation procedure and history[55,56], no comprehensive characterization of its composition and structure has yet been published. A previous study by Storm *et al.*[57] of the surface contamination on silicon wafers stored in wafers boxes indicated that the intensity of the ion species NH_4^+, $C_5H_{12}N^+$, $C_8H_5O_3^+$, and CH_3^+ increased almost linearly with time up to 6 days. The level of these contaminants significantly increased if the samples were stored in open boxes with laminar airflow over them. Similarly, Roche *et al.*[56], using a variety of different methods (*i.e.*, ellipsometry, water contact angle, infrared spectroscopy, thermal desorption coupled with ion mobility spectroscopy, thermal desorption coupled with gas chromatography-mass spectrometry, time-of-flight secondary ion mass spectroscopy (ToF-SIMS)), demonstrated that storage in closed containers reduces the contamination compared with the use of open ones. The ToF-SIMS results presented by Roche *et al.* also allowed the identification of the fragments of the molecular species adsorbed on silicon surfaces, *i.e.*, $SiC_3H_9^+$, $C_8H_5O_3^+$, Cl^-, F^-, SO_4^{2-}. A detailed investigation of the chemical nature of the adventitious contamination adsorbed on solid surfaces is particularly important for several research fields, since such contamination can have a substantial effect on surface properties including wettability and reactivity[58].
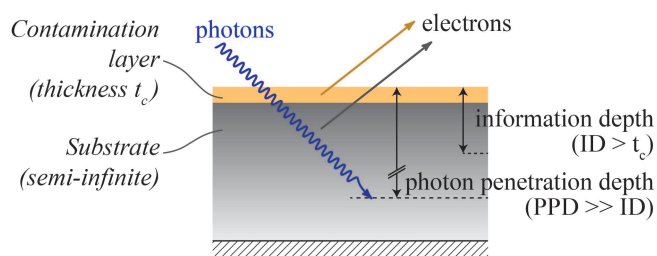
Figure 1. Schematic diagram of the near-surface structure of a substrate with an organic contamination layer (topmost layer). Since the information depth in X-ray photoelectron spectroscopy (XPS) and NEXAFS spectroscopy is larger than the thickness of the carbonaceous contamination layer (typically <2 nm[55]) and smaller than the photon penetration depth, the photoelectrons leaving the sample's near-surface region and measured by the detector originate from both the substrate and the contamination layer.

With X-ray photoelectron spectroscopy (XPS), the composition and thickness of each layer constituting a multilayer system can be determined without applying any destructive technique[53,54,59-65]. However, no methodology for extracting the photo-absorption spectrum of a single layer within a multilayer structure has ever been reported for NEXAFS spectroscopy in the literature.

Here, we present a novel analytical methodology for removing the contribution of thin overlayers (with thickness smaller than the information depth) from partial electron yield (PEY) NEXAFS spectra of two-layered systems (constituted by a substrate covered by an overlayer) to give the photo-absorption NEXAFS spectrum of the substrate. This method relies on the subtraction of the characteristic NEXAFS spectrum of the overlayer adsorbed on a reference surface from the spectrum of the two-layer system of interest once the thickness of both overlayers is determined by XPS. Compared to the "double normalization" method occasionally used in the literature to correct for the signal from carbon contamination[37], which assumed the

contamination layers on the specimen sample surface and on the reference sample surface to have the same thickness, composition, and density, the method here outlined accurately accounts for the different thickness of the overlayers on the reference sample and specimen of interest, while checking that their composition is not significantly different. The newly-developed approach is applied to NEXAFS experimental data acquired on air-exposed carbon-based materials (ultrananocrystalline diamond (UNCD) and hydrogenated amorphous carbon (a-C:H) films) and allowed for the removal of the contribution of adventitious carbon contamination from the as-acquired spectra to give the intrinsic photo-absorption NEXAFS spectra of these materials.

EXPERIMENTAL

To check the applicability of the formalism described in the manuscript, four carbon-based materials were investigated: hydrogen-terminated ultrananocrystalline diamond (UNCD Aqua 25, Advanced Diamond Technologies, Romeoville, IL US), and hydrogenated amorphous carbon (a-C:H) films (HGST, San Jose, CA, USA). The UNCD films (thickness: 1 μm) were deposited on a silicon wafer using hot filament chemical vapor deposition (HFCVD). The a-C:H films (thickness: 30 nm) were grown on glass disks coated with 20 nm of NiTa by plasma enhanced chemical vapor deposition (PECVD) from acetylene as gas precursor (NTI source, Intevac Inc., Santa Clara, CA, USA) using three different acceleration bias voltages (60, 120, and 180 V). The sample sizes were approximately 10x10 mm^2. All samples were cleaned with acetone and ethanol in laboratory air, dried with nitrogen, and stored for several weeks in a nitrogen-purged box before being exposed to laboratory air for 2 days, and then examined by X-ray photoelectron spectroscopy (XPS) and near-edge X-ray absorption fine structure (NEXAFS) spectroscopy.

To calculate the thickness and composition of the carbonaceous contamination layer adsorbed on these films, XPS measurements were performed. A detailed description of the experimental procedures for acquiring and processing the XPS data is reported in the Supporting Information.

Near-edge X-ray absorption fine structure (NEXAFS) spectroscopic measurements were performed at the NIST/Dow endstation of beamline U7A and at the Oak Ridge National Laboratory endstation of beamline U12A at the National Synchrotron Light Source (NSLS), Brookhaven National Laboratory (Upton, NY, USA). The photon source of these beamlines is a bending magnet, and covers an energy range from 180 to 1100 eV for U7A and from 100 to 800 eV for U12A. The photon flux is 2×10^{11} photons/second/0.1% bandwidth, and the resolution ($\Delta E/E$) is ~1×10^{-3}. All measurements were carried in partial electron yield (PEY) mode and at a photon incidence angle of 55° with respect to the sample surface (the so-called "magic angle") to suppress the effects related to the X-ray polarization[1]. For the experiments described here, the entrance grid bias (EGB) of the channeltron detector was set to -225 V at U7A and to -230 V at U12A to enhance surface sensitivity and minimize the detection of Auger electrons that suffered from energy loss while travelling through the sample before being emitted into the continuum. The monochromator energy was calibrated using the carbon K-edge-π^{*} transition of freshly-cleaved highly ordered pyrolytic graphite (HOPG, grade 2, SPI Supplies, West Chester, PA, USA), located at 285.5 eV. The spectra acquired at U7A were first normalized to the absorption current measured simultaneously from a gold mesh placed in the beamline upstream from the analysis chamber. As for the spectra acquired at U12A, they were first normalized to the absorption current measured under the same experimental conditions on a sputter-cleaned platinum sample. Since the analyses carried out at U7A and at U12A provided comparable results, only the spectra acquired at the former beamline are displayed in the present work.

The quantitative evaluation of the fraction of sp^2-bonded carbon in the specimens on the basis of NEXAFS data was performed using the procedure described in Ref. [36,66-68]. The methodology is based on the relative integrated intensity ratios of the C1s→π* and C1s→σ* peaks for the sample under investigation and for a reference specimen:

$$f_{sp^2} = \frac{I_{sam}^{\pi^*} I_{ref}(\Delta E)}{I_{sam}(\Delta E) I_{ref}^{\pi^*}}$$

Eq. 1

where $I_{sam}^{\pi^*}$ and $I_{ref}^{\pi^*}$ are, respectively, the areas of the C1s→π* peaks for the sample and reference, whereas $I_{sam}(\Delta E)$ and $I_{ref}(\Delta E)$ are the areas under the NEXAFS spectrum between 288.6 eV and 320 eV for the sample and reference, respectively. As a reference, the spectrum of a freshly-cleaved HOPG (100% sp^2-bonded carbon) sample was acquired with the X-ray beam incident at an angle of 45° to the sample surface to account for the cos^2(Θ) (Θ angle between the X-ray beam and the sample surface) angular dependence of the π* and σ* resonance intensity[1].

All the XPS and NEXAFS results reported here are mean values calculated from at least three independent measurements, with the corresponding standard deviation reported.

RESULTS AND DISCUSSION

According to the common mathematical formalism describing the emission of Auger electrons from a solid surface[1,69], the photoelectron signal intensity (I), which is proportional to the number of Auger electrons created throughout the sampling depth (N_e), can be expressed as:

$$I = \frac{\Omega}{4\pi} \int_0^\infty N_e \, dz = \frac{\Omega I_0 A_0}{4\pi \sin(\theta)} \int_0^\infty n_v(z) \sigma_E \exp\left(-\frac{z}{\lambda^* \cos\phi \cos\omega}\right) dz$$

Eq. 2

where Ω is the solid angle subtended by the electron detector, I_0 the incident photon flux density, A_0 the area irradiated by the incident X-rays, θ the angle between the surface and the incident X-

ray beam, $n_v(z)$ the number density of absorbing atoms, σ_E the absorption cross section (assumed to be independent of the angle between the transition dipole moment of the final orbital state of the excited atom and the electric field vector of the incident X-ray beam. This assumption is valid when analyzing disordered materials, as in the present case), λ^* the electron escape depth (EED), ϕ the electron emission angle (respect to the surface normal), and ω the angle that the electron detector makes with the plane defined by the incoming X-ray beam and the sample surface.

As shown in the full derivation in the Supporting Information, for a two-layered system in which both the overlayer and the substrate contain the same element i, where the overlayer thickness (t_{over}^{sub}) is smaller than the information depth at the l transition (e.g., K-edge) of the element i (e.g., carbon), and where the number density of absorbing atoms is constant both in the overlayer and in the substrate throughout the sampling depth, then the photoelectron signal can be expressed as:

$$I_{l,i,TOT} = I_{l,i,over} + I_{l,i,sub} = I_{l,i,over}^{\infty}\left[1 - \exp\left(-\frac{t_{over}^{sub}}{\lambda^* \cos\phi \cos\omega}\right)\right] + I_{l,i,sub}^{\infty} \exp\left(-\frac{t_{over}^{sub}}{\lambda^* \cos\phi \cos\omega}\right) \qquad \text{Eq. 3}$$

where $I_{l,i,sub}^{\infty}$ and $I_{l,i,over}^{\infty}$ are the signal intensities for a homogeneous, semi-infinite sample having the same composition and density of, respectively, the substrate and the overlayer. According to Equation 3, the intrinsic photo-absorption NEXAFS spectrum of the material under investigation ($I_{l,i,sub}^{\infty}$) can be computed from the NEXAFS spectrum of a two-layered system ($I_{l,i,TOT}$) once $I_{l,i,over}^{\infty}$, t_{over}^{sub}, λ^*, ϕ, and ω are known.

The angles ϕ and ω are set by the experimental configuration used for acquiring the spectra, and are thus known. However, the determination of the EED (λ^*) requires the knowledge of the

inelastic mean free path (λ) and its dependence on the entrance grid bias (EGB) of the channeltron photoelectron detector[14]. However, upon increasing the EGB voltage, the EED of the detected electrons can be approximated with the effective attenuation length of photoelectrons, which can be calculated from predictive formulas[70-74] or obtained from the NIST Electron Effective-Attenuation-Length Database for electron kinetic energy between 50 and 2000 eV[75].

The overlayer thickness t_{over}^{sub} can be determined in multiple ways. Secondary ion mass spectroscopy (SIMS) and depth profiling by Auger electron spectroscopy and XPS could provide an accurate estimate of the overlayer thickness, but these methods are destructive. Alternately, the overlayer thickness can be determined non-destructively by XPS[53,54,59-65]. Since most NEXAFS endstations at modern synchrotron facilities include XPS spectrometers, the calculation of the overlayer thickness can be performed by acquiring XPS spectra in the same experimental chamber, thus avoiding any risk of changing the composition and thickness of the contamination layer upon transferring the sample to a dedicated XPS chamber. Even if the employed NEXAFS endstation does not include a XPS spectrometer, XPS measurements can still be carried out separately with careful sample handling (in this case the XPS analyses should be performed before and after the NEXAFS measurements to check reproducibility).

The signal intensity for the overlayer $I_{l,i,over}^{\infty}$ can be determined from the NEXAFS spectrum acquired on a reference material covered with a thin overlayer having the same composition, structure, and density (but not necessarily thickness) of the overlayer present on the substrate under investigation. Such a computation requires that: a) the reference material does not contain the element i, whose transitions are investigated by NEXAFS spectroscopy; and b) the NEXAFS spectrum of the reference material in the photon range of the l transition of element i does not exhibit any absorption feature. The intensity of the signal originating from the presence of a thin

12

overlayer (with thickness t_{over}^{ref}, which is smaller than the information depth at the l transition of the element i) on the reference sample's surface can be expressed using Equation 3 as:

$$I_{l,i,over}^{ref} = \tilde{I}_{l,i,over}^{\infty} \left[1 - \exp\left(-\frac{t_{over}^{ref}}{\lambda^* \cos\phi \cos\omega} \right) \right] \qquad \text{Eq. 4}$$

where $\tilde{I}_{l,i,over}^{\infty}$ is the signal intensity coming from a homogeneous, semi-infinite sample having the same composition, structure, and density of the overlayer present on the reference sample surface.

Once t_{over}^{ref} is determined by XPS[53,54,59-65], the signal intensity $\tilde{I}_{l,i,over}^{\infty}$ can be calculated from Equation 4. If the composition (calculated by XPS) of the overlayers on the reference material and on the substrate under investigation are comparable, and assuming that the density of the overlayer on the reference material and on the substrate are not significantly different, the computed NEXAFS signal intensity $\tilde{I}_{l,i,over}^{\infty}$ can be equated to $I_{l,i,over}^{\infty}$ and used in Equation 3.

Therefore, the intrinsic photo-absorption NEXAFS spectrum of the material under investigation ($I_{l,i,sub}^{\infty}$) can be calculated as follows:

$$I_{l,i,sub}^{\infty} = A\left[I_{l,i,TOT} - B\, I_{l,i,over}^{ref} \right], \text{ where } A = \frac{1}{\exp\left(-\frac{t_{over}^{sub}}{\lambda^* \cos\phi \cos\omega} \right)} ; \quad B = \frac{1 - \exp\left(-\frac{t_{over}^{sub}}{\lambda^* \cos\phi \cos\omega} \right)}{1 - \exp\left(-\frac{t_{over}^{ref}}{\lambda^* \cos\phi \cos\omega} \right)} \qquad \text{Eq. 5}$$

The method was applied to NEXAFS experimental data acquired on carbon-based materials (ultrananocrystalline diamond (UNCD) and hydrogenated amorphous carbon (a-C:H) films), which were exposed to air for a prolonged period of time (this ensures that a thin carbonaceous contamination layer is present on the specimen surface).

The as-acquired C K-edge PEY NEXAFS spectra of UNCD and a-C:H films are displayed in Figure 2 together with the NEXAFS spectrum of the carbonaceous contamination layer adsorbed

on a reference gold specimen. All spectra exhibit an absorption feature at 285.0±0.1 eV, which is due to the C1s→π^* transition for disordered carbon-carbon bonds[1]. The intensity of this peak directly correlates with the fraction of sp^2-bonded carbon in the near surface region. For a-C:H films, the NEXAFS spectra are characterized by a broad hump between 288 and 305 eV (which is due to the C1s→σ^* transition for disordered carbon-carbon bonds[1,42,76]), whereas the spectrum of UNCD exhibits sharper C1s→σ^* transitions that are characteristic of ordered sp^3-hybridized carbon-carbon bonds, namely the edge jump at ~289 eV, the exciton peak at ~289.3 eV, and the second band gap at 303 eV[13]. The presence of significant amounts of hydrogen in a-C:H films and the hydrogen-termination of UNCD also resulted in the detection of a shoulder at ~287.0 eV (for a-C:H) and ~287.5 eV (for UNCD), which can be assigned to the C1s→σ^* transition for C-H bonds[1]. The observed shift of the characteristic C-H absorption feature between the spectra of a-C:H and the spectrum of UNCD may be due to the different bonding states in these materials: while hydrogen terminates primarily sp^3-bonded carbon atoms at the UNCD surface, it is present in a range of bonding environments within the bulk of a-C:H films. Due to the sample exposure to air before the NEXAFS analysis, a broad absorption feature was detected at 288.5-289.3 eV and could be assigned to the C-O σ^* antibonding orbital[77]. The presence of carbonyl groups on the sample surface could also contribute to the spectral intensity between 286.7 and 288.5 eV (C1s→π^* transition)[1,68].
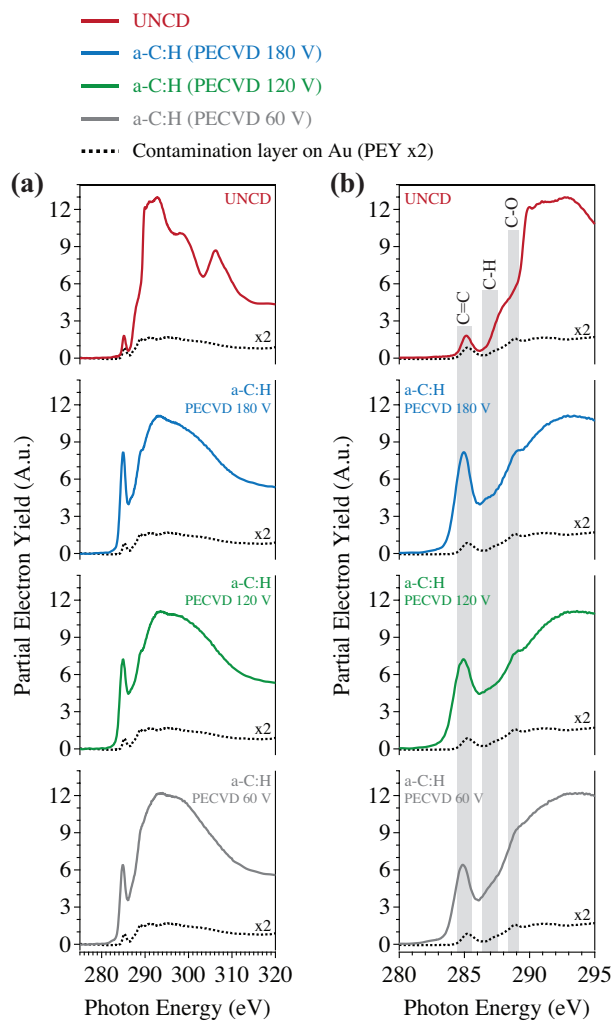
Figure 2. Carbon K-edge NEXAFS spectra acquired at beamline U7A (NSLS) on gold, ultrananocrystalline diamond (UNCD), and hydrogenated amorphous carbon (a-C:H) films grown by plasma enhanced chemical vapor deposition (PECVD) with different acceleration bias voltages (60, 120, and 180 V). (a) Whole photon energy scale; (b) zoomed absorption edge region. All spectra are pre-edge normalized.

Since the procedure outlined above requires the knowledge of the thickness of the overlayer present on both the specimen and the reference material, and is applicable only if the composition of that overlayer is similar in both cases, XPS analyses were performed on the

carbon-based films as well as on the reference gold sample to check for the consistency of the contamination layer's composition. A detailed description of the XPS results is reported in the Supporting Information. The results show that the composition of the contamination layers adsorbed on gold was similar to those on the carbon-based materials under investigation (Table S.1). Furthermore, the area ratio of the peaks contributing to the carbon 1s XPS signal (namely aliphatic carbon, C-O, C=O, and O-C=O) was not significantly different between the specimens, thus suggesting a comparable carbon bonding configuration in the contamination layer independent of the substrate. Since the XPS measurements were carried out in a dedicated chamber, the acquisition of XPS spectra was performed both before and after the NEXAFS analysis: in all cases, no significant variations in the composition and thickness of the carbonaceous contamination layer were observed.

The XPS measurements of overlayer thickness thus allowed the method to be applied. The intrinsic photo-absorption NEXAFS spectrum ($I_{l,i,sub}^{\infty}$) of the materials under investigation (*i.e.*, UNCD and a-C:H films) computed from Equation 5 are displayed in Figure 3a together with the as-acquired (*i.e.*, non-corrected) spectra. Upon correcting for the contribution of the thin carbonaceous contamination layer from the as-acquired spectra, the calculated intensity above the absorption edge increases. This enhancement of the post-edge intensity derives from eliminating the attenuation of the overlayer on the photoelectron signal arising from the sample. This is in agreement with the work of Sohn *et al.*[69], who showed that the post-edge intensity of the substrate signal decreases with the adsorbate thickness.

To compare the as-acquired with corrected NEXAFS spectra, a pre- and post-edge normalization was performed (Figure 3b and 3c). In this way, variations in spectral intensity only arise from chemical changes and are independent of the total carbon content. On the basis of

XPS and NEXAFS measurements, the carbonaceous contamination layer can be described as a layer containing carbon and oxygen ([O]/[C]=0.11±0.02) with an approximate thickness of 0.6 nm and a sp^2-bonded carbon fraction of 0.19±0.03. Upon removing the contribution from this layer, the intensity of the C1s→π^* transition for disordered carbon-carbon bonds[1] at 285.0±0.1 eV slightly decreased in the case of UNCD, whereas it increased for a-C:H films. Very significantly, for the a-C:H films, the broad absorption feature at 288.5-289.3 eV (assigned to the C-O σ^* antibonding orbital[77]) was greatly reduced. The spectral changes induced by the removal of the contribution of the carbonaceous contamination from the as-acquired data substantially affected the computation of the carbon hybridization state. Upon ignoring the presence of a contamination layer, $i.e.$, under the assumption of structural and compositional homogeneity within the probed volume, the fraction of sp^2-bonded carbon was 0.062±0.001 for UNCD, 0.315±0.003 for a-C:H (60 V), 0.489±0.002 for a-C:H (120 V), and 0.493±0.003 for a-C:H (180 V). Correcting the spectra for the contribution of adventitious contamination yielded significantly different values: 0.069±0.001 for UNCD, 0.341±0.003 for a-C:H (60 V), 0.521±0.002 for a-C:H (120 V), and 0.527±0.003 for a-C:H (180 V).

Further NEXAFS analyses were performed on a-C:H (180 V) using a second synchrotron endstation (U12A) with a different spectrometer configuration. The larger angle between the PEY detector and the sample surface at U12A (50°) compared to the same angle at U7A (10°) resulted in a reduction of the information depth, $i.e.$, 2.5 nm at U12A vs. 3.8 nm at U7A. Even though the fraction of sp^2-hybridized carbon computed from the uncorrected spectra acquired at U12A (0.415±0.005) significantly differs from the fraction calculated from the uncorrected spectra acquired at U7A (0.493±0.003), upon removing the contribution of the adventitious

carbonaceous contamination the two independent series of analyses yield numerical results that are within the uncertainty of the measurements (0.521±0.005 (U12A) *vs*. 0.527±0.003 (U7A)).

These findings demonstrate that: a) significant errors (estimated to be between 5 and 20% from the data presented here) can be introduced in the computation of the carbon hybridization state from NEXAFS spectra if the contribution from the carbonaceous contamination layer is not removed; and b) the assumption of structural and compositional homogeneity within the nanometer-depth scale probed by NEXAFS spectroscopy can be misleading when analyzing specimens with surface layers.

Finally, it is important to emphasize that amorphous carbon-based materials can possess a near-surface region whose structure is significantly different from that of the bulk of the material, depending on the synthesis and growth conditions[78]. Since NEXAFS spectroscopy probes a nanometer-scale depth, the structural information gained by this analytical method can potentially differ from the outcomes of analyses carried out with techniques having different information depths (such as Raman spectroscopy, XPS, and X-ray-induced Auger electron spectroscopy (XAES)). The comparison between the NEXAFS results presented herein with the outcomes of Raman[79], XPS, and XAES measurements, which will be the subject of a separate publication, provides clear experimental evidence of the presence of structurally-different near-surface regions on certain hydrogenated amorphous films: such a conclusion could not have been definitively reached without first correcting for the contamination layer using the method presented here.

CONCLUSIONS

A novel method was developed for accurately removing the contribution of thin overlayers (with thickness smaller than the information depth) from NEXAFS spectra of two-layered systems to reveal the photo-absorption NEXAFS spectrum of the substrate. This new and generally-applicable approach was used for processing NEXAFS data acquired on air-exposed carbon-based materials, namely UNCD and a-C:H films, and allowed for the removal of the contribution of the adventitious carbon contamination adsorbed on the sample's surfaces from the as-acquired NEXAFS C K-edge spectra. The resulting spectra provided qualitatively distinct interpretations and quantitatively distinct values regarding the sample's composition and bonding.

This novel method opens a new path for processing NEXAFS spectra without the assumption of chemical and structural homogeneity down to the depth probed by this surface-analytical method and allows avoiding the large errors that this assumption might introduce when analyzing multilayer structures.
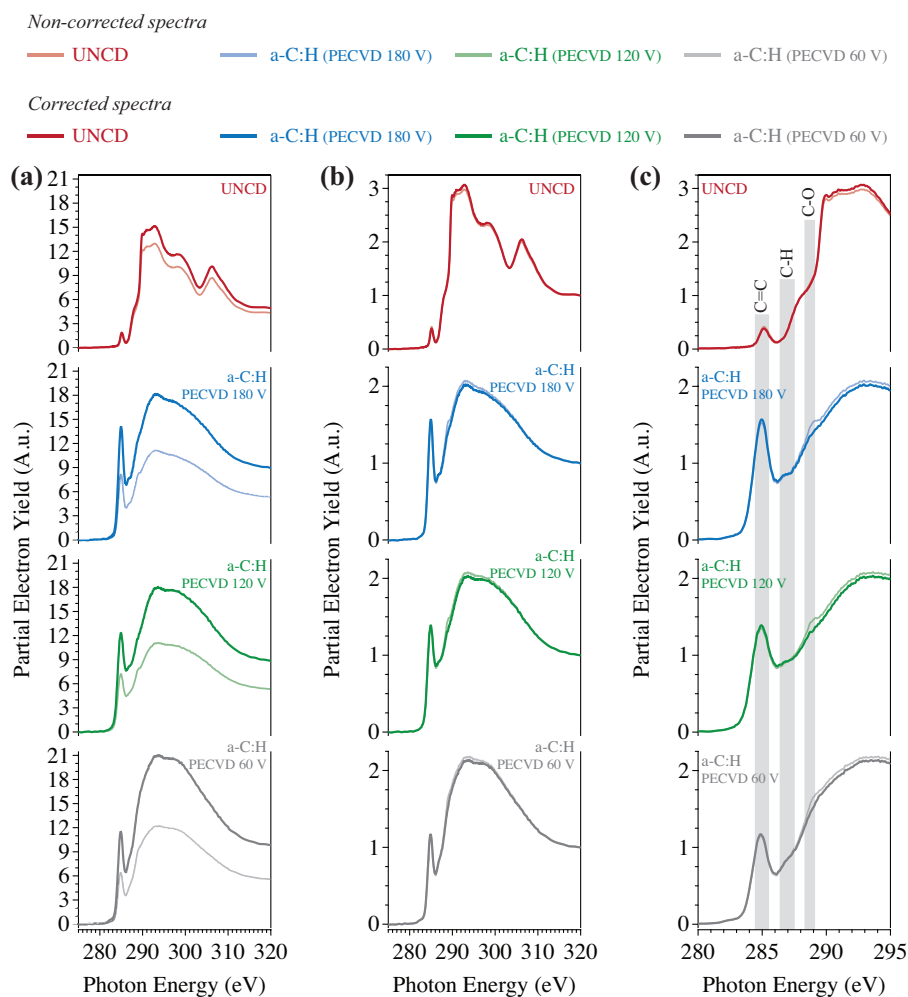
Figure 3. Carbon K-edge NEXAFS spectra acquired at beamline U7A (NSLS) – before and after the correction for the presence of a carbonaceous contamination layer – of UNCD and a-C:H films grown by PECVD with different acceleration bias voltages (60, 120, and 180 V). (a) pre-edge normalized spectra (whole photon energy scale); (b) pre- and post-edge normalized spectra (whole photon energy scale); (c) pre- and post-edge normalized spectra (zoomed absorption edge region).

ASSOCIATED CONTENT

Supporting Information. A detailed description of the experimental procedures for acquiring and processing the XPS data is reported. The results of the XPS analysis performed on UNCD, a-C:H films, and a gold reference specimen are also presented. This material is available free of charge via the Internet at http://pubs.acs.org.

AUTHOR INFORMATION

Corresponding Author

*Email: carpick@seas.upenn.edu

Notes

The authors declare no competing financial interests.

REFERENCES

(1) Stöhr, J. *NEXAFS Spectroscopy*. Springer-Verlag: 1992; p. 403.

(2) Anders, S.; Padmore, H. A.; Duarte, R. M.; Renner, T.; Stammler, T.; Scholl, A.; Scheinfein, M. R.; Stöhr, J.; Séve, L.; Sinkovic, B. *Review of Scientific Instruments* **1999**, *70*, 3973-3981.

(3) Bauer, E.; Mundschau, M.; Swiech, W.; Telieps, W. *Ultramicroscopy* **1989**, *31*, 49-57.

(4) Engel, W.; Kordesch, M. E.; Rotermund, H. H.; Kubala, S.; von Oertzen, A. *Ultramicroscopy* **1991**, *36*, 148-153.

(5) Renault, O.; Barrett, N.; Bailly, A.; Zagonel, L. F.; Mariolle, D.; Cezar, J. C.; Brookes, N. B.; Winkler, K.; Krömker, B.; Funnemann, D. *Surface Science* **2007**, *601*, 4727-4732.

(6) Konicek, A. R.; Jaye, C.; Hamilton, M. A.; Sawyer, W. G.; Fischer, D. A.; Carpick, R. W. *Tribology Letters* **2011**, *44*, 99-106.

(7) Lindsay, R.; Thornton, G. *Topics in Catalysis* **2002**, *18*, 15-19.

(8) Bauer, M.; Gastl, C. *Physical Chemistry Chemical Physics* **2010**, *12*, 5575-5584.

(9) Ramaker, D. E.; Koningsberger, D. C. *Physical Chemistry Chemical Physics* **2010**, *12*, 5514-5534.

(10) MacNaughton, J. B.; Naslund, L.-A.; Anniyev, T.; Ogasawara, H.; Nilsson, A. *Physical Chemistry Chemical Physics* **2010**, *12*, 5712-5716.

(11) Anniyev, T.; Ogasawara, H.; Ljungberg, M. P.; Wikfeldt, K. T.; MacNaughton, J. B.; Naslund, L.-A.; Bergmann, U.; Koh, S.; Strasser, P.; Pettersson, L. G. M.; Nilsson, A. *Physical Chemistry Chemical Physics* **2010**, *12*, 5694-5700.

(12) Nicholls, M.; Najman, M. N.; Zhang, Z.; Kasrai, M.; Norton, P. R.; Gilbert, P. U. P. A. *Canadian Journal of Chemistry* **2007**, *85*, 816-830.

(13) Konicek, A. R.; Grierson, D. S.; Gilbert, P. U. P. A.; Sawyer, W. G.; Sumant, A. V.; Carpick, R. W. *Physical Review Letters* **2008**, *100*, 235502.

(14) Genzer, J.; Kramer, E. J.; Fischer, D. A. *Journal of Applied Physics* **2002**, *92*, 7070-7079.

(15) Gliboff, M.; Sang, L.; Knesting, K. M.; Schalnat, M. C.; Mudalige, A.; Ratcliff, E. L.; Li, H.; Sigdel, A. K.; Giordano, A. J.; Berry, J. J.; Nordlund, D.; Seidler, G. T.; Brédas, J.-L.; Marder, S. R.; Pemberton, J. E.; Ginger, D. S. *Langmuir* **2013**, *29*, 2166-2174.

(16) Cheng, F.; Gamble, L. J.; Castner, D. G. *Analytical Chemistry* **2008**, *80*, 2564-2573.

(17) Turgman-Cohen, S.; Fischer, D. A.; Kilpatrick, P. K.; Genzer, J. *ACS Applied Materials & Interfaces* **2009**, *1*, 1347-1357.

(18) Hemraj-Benny, T.; Banerjee, S.; Sambasivan, S.; Balasubramanian, M.; Fischer, D. A.; Eres, G.; Puretzky, A. A.; Geohegan, D. B.; Lowndes, D. H.; Han, W.; Misewich, J. A.; Wong, S. S. *Small* **2006**, *2*, 26-35.

(19) Winter, A. D.; Larios, E.; Alamgir, F. M.; Jaye, C.; Fischer, D. A.; Campo, E. M. *Langmuir* **2013**, *29*, 15822-15830.

(20) Breuer, T.; Witte, G. *ACS Applied Materials & Interfaces* **2013**, *5*, 9740-9745.

(21) Lee, H.-J.; Lee, K.-S.; Cho, J.-M.; Lee, T.-S.; Kim, I.; Jeong, D. S.; Lee, W.-S. *ACS Applied Materials & Interfaces* **2013**, *5*, 11631-11640.

(22) Li, Y. S.; Tang, Y.; Yang, Q.; Maley, J.; Sammynaiken, R.; Regier, T.; Xiao, C.; Hirose, A. *ACS Applied Materials & Interfaces* **2010**, *2*, 335-338.

(23) Sankaran, K. J.; Lin, Y.-F.; Jian, W.-B.; Chen, H.-C.; Panda, K.; Sundaravel, B.; Dong, C.-L.; Tai, N.-H.; Lin, I. N. *ACS Applied Materials & Interfaces* **2013**, *5*, 1294-1301.

(24) Saravanan, A.; Huang, B.-R.; Sankaran, K. J.; Kunuku, S.; Dong, C.-L.; Leou, K.-C.; Tai, N.-H.; Lin, I. N. *ACS Applied Materials & Interfaces* **2014**, *6*, 10566-10575.

(25) Yeap, W. S.; Liu, X.; Bevk, D.; Pasquarelli, A.; Lutsen, L.; Fahlman, M.; Maes, W.; Haenen, K. *ACS Applied Materials & Interfaces* **2014**, *6*, 10322-10329.

(26) Zhong, S.; Zhong, J. Q.; Mao, H. Y.; Wang, R.; Wang, Y.; Qi, D. C.; Loh, K. P.; Wee, A. T. S.; Chen, Z. K.; Chen, W. *ACS Applied Materials & Interfaces* **2012**, *4*, 3134-3140.

(27) Kikuma, J.; Tonner, B. P. *Journal of Electron Spectroscopy and Related Phenomena* **1996**, *82*, 53-60.

(28) Watts, B.; Swaraj, S.; Nordlund, D.; Lüning, J.; Ade, H. *The Journal of Chemical Physics* **2011**, *134*, 024702.

(29) Ade, H.; Hitchcock, A. P. *Polymer* **2008**, *49*, 643-675.

(30) Park, D.; Finlay, J. A.; Ward, R. J.; Weinman, C. J.; Krishnan, S.; Paik, M.; Sohn, K. E.; Callow, M. E.; Callow, J. A.; Handlin, D. L.; Willis, C. L.; Fischer, D. A.; Angert, E. R.; Kramer, E. J.; Ober, C. K. *ACS Applied Materials & Interfaces* **2010**, *2*, 703-711.

(31) Sundaram, H. S.; Cho, Y.; Dimitriou, M. D.; Finlay, J. A.; Cone, G.; Williams, S.; Handlin, D.; Gatto, J.; Callow, M. E.; Callow, J. A.; Kramer, E. J.; Ober, C. K. *ACS Applied Materials & Interfaces* **2011**, *3*, 3366-3374.

(32) Tillack, A. F.; Noone, K. M.; MacLeod, B. A.; Nordlund, D.; Nagle, K. P.; Bradley, J. A.; Hau, S. K.; Yip, H.-L.; Jen, A. K. Y.; Seidler, G. T.; Ginger, D. S. *ACS Applied Materials & Interfaces* **2011**, *3*, 726-732.

(33) Konicek, A. R.; Grierson, D. S.; Sumant, A. V.; Friedmann, T. A.; Sullivan, J. P.; Gilbert, P. U. P. A.; Sawyer, W. G.; Carpick, R. W. *Physical Review B* **2012**, *85*, 155448.

(34) Morar, J. F.; Himpsel, F. J.; Hollinger, G.; Hughes, G.; Jordan, J. L. *Physical Review Letters* **1985**, *54*, 1960-1963.

(35) Ray, S. C.; Erasmus, R. M.; Tsai, H.; nbsp; M; Pao, C.; W; Lin, I. N.; Pong, W.; F. *Japanese Journal of Applied Physics*, *51*, 095201.

(36) Sumant, A. V.; Gilbert, P. U. P. A.; Grierson, D. S.; Konicek, A. R.; Abrecht, M.; Butler, J. E.; Feygelson, T.; Rotter, S. S.; Carpick, R. W. *Diamond and Related Materials* **2007**, *16*, 718-724.

(37) Sumant, A. V.; Grierson, D. S.; Gerbi, J. E.; Birrell, J.; Lanke, U. D.; Auciello, O.; Carlisle, J. A.; Carpick, R. W. *Advanced Materials* **2005**, *17*, 1039-1045.

(38) Sumant, A. V.; Grierson, D. S.; Gerbi, J. E.; Carlisle, J. A.; Auciello, O.; Carpick, R. W. *Physical Review B* **2007**, *76*, 235429.

(39) Anders, S.; Stammler, T.; Fong, W.; Bogy, D. B.; Bhatia, C. S.; Stöhr, J. *Journal of Vacuum Science & Technology A: Vacuum, Surfaces, and Films* **1999**, *17*, 2731-2736.

(40) Diaz, J.; Anders, S.; Zhou, X.; Moler, E. J.; Kellar, S. A.; Hussain, Z. *Journal of Electron Spectroscopy and Related Phenomena* **1999**, *101-103*, 545-550.

(41) Gago, R.; Jimenez, I.; Albella, J. M.; Climent-Font, A.; Caceres, D.; Vergara, I.; Banks, J. C.; Doyle, B. L.; Terminello, L. J. *Journal of Applied Physics* **2000**, *87*, 8174-8180.

(42) Grierson, D. S.; Sumant, A. V.; Konicek, A. R.; Friedmann, T. A.; Sullivan, J. P.; Carpick, R. W. *Journal of Applied Physics* **2010**, *107*, 033523-033525.

(43) Lenardi, C.; Piseri, P.; Briois, V.; Bottani, C. E.; Bassi, A. L.; Milani, P. *Journal of Applied Physics* **1999**, *85*, 7159-7167.

(44) Ray, S. C.; Tsai, H. M.; Chiou, J. W.; Bose, B.; Jan, J. C.; Krishna, K.; Pong, W. F.; Dasgupta, D.; Tsai, M. H. *Journal of Physics: Condensed Matter* **2004**, *16*, 5713.

(45) Saikubo, A.; Yamada, N.; Kanda, K.; Matsui, S.; Suzuki, T.; Niihara, K.; Saitoh, H. *Diamond and Related Materials* **2008**, *17*, 1743-1745.

(46) Wesner, D.; Krummacher, S.; Carr, R.; Sham, T. K.; Strongin, M.; Eberhardt, W.; Weng, S. L.; Williams, G.; Howells, M.; Kampas, F.; Heald, S.; Smith, F. W. *Physical Review B* **1983**, *28*, 2152-2156.

(47) Schultz, B. J.; Patridge, C. J.; Lee, V.; Jaye, C.; Lysaght, P. S.; Smith, C.; Barnett, J.; Fischer, D. A.; Prendergast, D.; Banerjee, S. *Nat Commun* **2011**, *2*, 372.

(48) Pacilé, D.; Papagno, M.; Rodríguez, A. F.; Grioni, M.; Papagno, L.; Girit, Ç. Ö.; Meyer, J. C.; Begtrup, G. E.; Zettl, A. *Physical Review Letters* **2008**, *101*, 066806.

(49) Maruyama, T.; Ishiguro, Y.; Nartitsuka, S.; Norimatsu, W.; Kusunoki, M.; Amemiya, K.; Ishii, H.; Ohta, T. *Japanese Journal of Applied Physics*, *51*, 055102.

(50) Maruyama, T.; Sakakibara, S.; Naritsuka, S.; Amemiya, K. *Diamond and Related Materials* **2011**, *20*, 1325-1328.

(51) Schöll, A.; Zou, Y.; Schmidt, T.; Fink, R.; Umbach, E. *Journal of Electron Spectroscopy and Related Phenomena* **2003**, *129*, 1-8.

(52) Watts, B.; Thomsen, L.; Dastoor, P. C. *Journal of Electron Spectroscopy and Related Phenomena* **2006**, *151*, 105-120.

(53) Olla, M.; Navarra, G.; Elsener, B.; Rossi, A. *Surface and Interface Analysis* **2006**, *38*, 964-974.

(54) Scorciapino, M. A.; Navarra, G.; Elsener, B.; Rossi, A. *The Journal of Physical Chemistry C* **2009**, *113*, 21328-21337.

(55) Seah, M. *J. Vac. Sci. Technol. A* **2003**, *21*, 345.

(56) Roche, A.; Wyon, C.; Marthon, S.; Ple, J. F.; Olivier, M.; Rochat, N.; Chabli, A.; Danel, A.; Juhel, M.; Tardif, F. *AIP Conference Proceedings* **2001**, *550*, 297-301.

(57) Storm, W.; Vandervorst, W.; Alay, J.; Meuris, M.; Opdebeeck, A.; Heynes, M. M. In *Proceedings of the Second International Symposium on Ultra-Clean Processing of Silicon Surfaces (UCPSS)*, Heyns, M., Ed., 1995, pp 367-370.

(58) Li, Z.; Wang, Y.; Kozbial, A.; Shenoy, G.; Zhou, F.; McGinley, R.; Ireland, P.; Morganstein, B.; Kunkel, A.; Surwade, S. P.; Li, L.; Liu, H. *Nat Mater* **2013**, *12*, 925-931.

(59) De Filippo, D.; Rossi, A.; Elsener, B.; Virtanen, S. *Surface and Interface Analysis* **1990**, *15*, 668-674.

(60) Elsener, B.; Rossi, A. *Materials Science Forum* **1995**, *192-194*, 225-236.

(61) Rossi, A.; Eisener, B. *Surface and Interface Analysis* **1992**, *18*, 499-504.

(62) Champaneria, R.; Mack, P.; White, R.; Wolstenholme, J. *Surface and Interface Analysis* **2003**, *35*, 1028-1033.

(63) Chang, J. P.; Green, M. L.; Donnelly, V. M.; Opila, R. L.; Eng, J.; Sapjeta, J.; Silverman, P. J.; Weir, B.; Lu, H. C.; Gustafsson, T.; Garfunkel, E. *Journal of Applied Physics* **2000**, *87*, 4449-4455.

(64) Opila, R. L.; Eng Jr, J. *Progress in Surface Science* **2002**, *69*, 125-163.

(65) Smith, G. C.; Livesey, A. K. *Surface and Interface Analysis* **1992**, *19*, 175-180.

(66) Gago, R.; Jiménez, I.; Albella, J. M.; Climent-Font, A.; Cáceres, D.; Vergara, I.; Banks, J. C.; Doyle, B. L.; Terminello, L. J. *Journal of Applied Physics* **2000**, *87*, 8174-8180.

(67) Kulik, J.; Lempert, G. D.; Grossman, E.; Marton, D.; Rabalais, J. W.; Lifshitz, Y. *Physical Review B* **1995**, *52*, 15812-15822.

(68) Osswald, S.; Yushin, G.; Mochalin, V.; Kucheyev, S. O.; Gogotsi, Y. *Journal of the American Chemical Society* **2006**, *128*, 11635-11642.

(69) Sohn, K. E.; Dimitriou, M. D.; Genzer, J.; Fischer, D. A.; Hawker, C. J.; Kramer, E. J. *Langmuir* **2009**, *25*, 6341-6348.

(70) Tanuma, S. In *Surface Analysis by Auger and X-Ray Photoelectron Spectroscopy*, Briggs, D.; Grant, J. T., Eds.; IM Publications: Chichester (UK), 2003, p. 259-294.

(71) Jablonski, A.; Powell, C. J. *Journal of Alloys and Compounds* **2004**, *362*, 26-32.

(72) Jablonski, A.; Powell, C. J. *Journal of Vacuum Science & Technology A* **2009**, *27*, 253-261.

(73) Powell, C. J.; Jablonski, A. *Nuclear Instruments and Methods in Physics Research Section A: Accelerators, Spectrometers, Detectors and Associated Equipment* **2009**, *601*, 54-65.

(74) Powell, C. J.; Jablonski, A. *Journal of Electron Spectroscopy and Related Phenomena* **2010**, *178–179*, 331-346.

(75) Powell, C. J.; Jablonski, A.; U.S. Department of Commerce, National Institute of Standards and Technology, Gaithersburg, MD, 2003.

(76) Comelli, G.; Stöhr, J.; Robinson, C. J.; Jark, W. *Physical Review B* **1988**, *38*, 7511-7519.

(77) Ishii, I.; Hitchcook, A. P. *Journal of Electron Spectroscopy and Related Phenomena* **1988**, *46*, 55-84.

(78) Wang, N.; Komvopoulos, K. *Journal of Materials Research* **2013**, *28*, 2124-2131.

(79) Rose, F.; Wang, N.; Smith, R.; Xiao, Q.-F.; Inaba, H.; Mastumura, T.; Matsumoto, H.; Dai, Q.; Marchon, B.; Mangolini, F.; Carpick, R. W. *Journal of Applied Physics* **2014**, *116*, 123516.

For TOC only

Carbon K-edge NEXAFS